THE JOURNAL OF PHYSICAL CHEMISTRY C

pubs.acs.org/JPCC Article

Transport and Interfacial Properties of Mixed Molten Carbonate/Hydroxide Electrolytes by Molecular Dynamics Simulations

Published as part of The Journal of Physical Chemistry virtual special issue "Emily A. Carter Festschrift".

Anirban Mondal, Jeffrey M. Young, Timothy A. Barckholtz, Gabor Kiss, Lucas Koziol,* and Athanassios Z. Panagiotopoulos*

Cite This: *J. Phys. Chem. C* 2020, 124, 23532−23540 Read Online

ACCESS | Metrics & More | Article Recommendations | Supporting Information

ABSTRACT: We use molecular dynamics simulations based on a recently developed force field to obtain the viscosity, ionic conductivity, and liquid−vapor surface tension of molten alkali-metal carbonate−hydroxide mixtures over a range of cation and hydroxide compositions. Recent experimental and simulation studies have suggested that molten carbonates contain non-negligible amounts of hydroxide ions in the presence of water at low partial pressures of CO_2. However, due to the high temperatures (≃600 °C or higher) required to melt pure alkali carbonates and their mixtures, there is a lack of experimental thermodynamic and transport data for these molten phases. Here, we deploy a recently parametrized force field for molten alkali carbonates and hydroxides [*J. Chem. Theory Comput.* **2020**, *16*, 5736−5746, DOI: 10.1021/acs.jctc.0c00285] to simulate some physical properties using atomistic molecular dynamics. Our predictions show a consistent decrease in viscosity and an increase in ionic conductivity with increasing hydroxide fractions, whereas a higher Li^+ mole fraction leads to an increase in both viscosity and ionic conductivity. The computed surface tension values exhibit an upward trend with higher asymmetry in cation and anion sizes. Structural analysis suggests that in the carbonate−hydroxide melts the smaller/harder ions, OH^- and Li^+, are more favored at the interface than the larger/softer ions, CO_3^{2-} and K^+/Na^+. The current approach provides a systematic route to obtaining physicochemical properties of molten alkali carbonate and hydroxide mixtures over a large domain of chemical compositions and thus can steer future experimental research for molten carbonates and their applications.

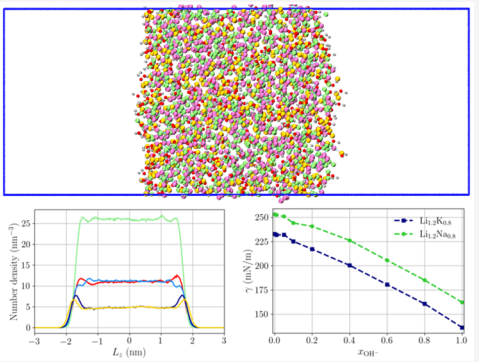

INTRODUCTION

Molten carbonates and their eutectic mixtures are interesting for multiple applications, such as heat transfer or storage media, and as ionic conductors in molten carbonate fuel cells (MCFCs).[1] Li-based alkali carbonate eutectics are already in commercial use in MCFCs for power generation.[2] More recently, MCFCs have also been explored for carbon capture to reduce CO_2 emission when using fossil fuels. The advantage of MCFCs is their ability to generate electricity with high (over 60%) fuel-to-energy conversion efficiency[3,4] while concentrating CO_2 across the fuel cell for later sequestration or utilization. In MCFCs, CO_2 is oxidized to a carbonate (CO_3^{2-}) ion at the cathode. The carbonate ion is then transported through the molten alkali-metal carbonate electrolyte to the anode side, where it is reduced by hydrogen and CO_2 is released into the anode gas stream. The high thermodynamic driving force of the overall reaction enables high CO_2 capture efficiency at the cathode while enriching it on the anode side.[5] While MCFCs are highly effective in carbon capture, the technology needs to be adapted to driving cathode CO_2 concentrations to very low levels in the presence of significant water concentrations.[6]

The overall efficiency of MCFCs is strongly impacted by the properties of the electrolyte, which mediates the dissolution of CO_2 and O_2 from the flue gas, the subsequent migration of carbonate ions across the cell, and wetting of the electrodes. Typically, an MCFC electrolyte is comprised of a mixture of Li/K or Li/Na carbonates near their eutectic compositions. These mixtures exhibit melting points 200−300 °C below that of the pure carbonates, allowing MCFCs to operate at lower temperatures, around 600 °C. Our recent results based on chemical reaction equilibrium simulations have revealed that, surprisingly, these carbonates contain substantial fractions of hydroxide ions provided the partial pressure of CO_2 is low

Received: August 10, 2020
Revised: September 18, 2020
Published: October 15, 2020

compared to that of H_2O.[7] Under CO_2-capture conditions, these hydroxides displace carbonate ions via the carbonate hydrolysis equilibrium, $CO_3^{2-}(l) + H_2O(g) \leftrightarrow 2OH^-(l) + CO_2(g)$. These findings have qualitatively explained the discrepancy between the charge and carbonate transfer balances in MCFCs reported in an experimental work by Rosen et al.[8]

Experimental investigations of physicochemical properties of molten carbonates under ambient pressure appeared a few decades ago.[9] However, due to the high temperatures of these melts, it is very difficult to obtain accurate data of the relevant properties, such as viscosity, conductivity, and surface tension, from experiments that often require special devices adapted to the measurement of a single observable. Molecular dynamics (MD) simulations are a useful tool for predicting multiple physical and transport properties, including under extreme conditions. An MD simulation relies on the knowledge of appropriate potentials describing the interatomic interactions for the system under consideration. One possibility of acquiring such potentials is via solving the electronic Schrödinger equation on-the-fly during each MD step, known as first-principles MD. Recently, first-principles MD simulations employing orbital-free (OF)[10] density functional theory (DFT) have been shown as a promising approach in the prediction of structural and dynamic properties of liquid metals.[11] However, this approach is more computationally demanding than classical MD that can access a broader temperature range and longer time scales. In classical MD simulations, on the contrary, the interatomic interactions are described via an empirical form of the potential known as force fields. These force fields can be derived by fitting to electronic structure calculations and/or available experimental data.

The first attempt to model molten carbonates using classical MD was initiated by Janssen and Tissen[12] for the unary Li_2CO_3, Na_2CO_3, and K_2CO_3 salts. There have been several subsequent studies using slightly modified versions of the Janssen–Tissen force field[13−18] that reported on the local structure, density, and transport properties of molten alkali-metal carbonates and their binary mixtures. More recently, Vuilleumier et al.[19] developed an empirical force field based on first-principle MD calculations that can predict the properties of molten $CaCO_3$ at a wide range of state points. In a similar approach, Corradini et al.[20] and Desmaele et al.[21] have parametrized models for molten alkali-metal carbonates and investigated the thermodynamic, structural, and transport properties of these salts over a range of compositions and state points. However, these models are restricted in composition to carbonates of single or multiple alkali-metals without the presence of other anions. To our knowledge, there has been no computational study of the physicochemical properties of mixed carbonate–hydroxide melts observed at certain conditions in MCFC systems.

Recently, we have reported a new force field parametrization which describes both carbonates and hydroxides with a consistent potential energy functional form.[22] The parameters were obtained by a genetic algorithm to fit both density and radial distribution functions (RDFs) obtained from first-principles MD and experimental vaporization enthalpies. The force field accurately predicts both chemical potential and density of the liquid phase. Although the predicted ion dynamics were found to be systematically slower than in experiments, the deviation in transport properties was consistent across different systems. An important feature of this force field is that its parameters can be extended to molten carbonate–hydroxide mixtures using standard combining rules.[23,24] Therefore, this force field can be employed to investigate the thermodynamic and transport properties of molten carbonate–hydroxide mixtures across a range of compositions. MD simulations provide insightful information on trends in the structural and transport quantities for these mixtures, and can guide and explain experimental studies. This forms the motivation for the present work.

Here, we report the transport and interface properties of viscosity, ionic conductivity, and surface tension in cation mixtures of molten alkali-metal carbonates, hydroxides, and carbonate–hydroxide systems. The content of this paper is organized as follows: After this introduction, we describe the computational details of the classical MD simulations. Next, we highlight the obtained results from the simulations and provides a comparison to the available experimental data. The final section presents our conclusions.

METHODS

Molecular models for carbonate, hydroxide, and the cations were taken from Mondal et al.[22] The models consist of Buckingham potentials to represent the van der Waals interactions and full charges on the cations and anions to represent the Coulomb interactions. We note that full charges were necessary to accurately reproduce the vaporizations enthalpies, as discussed in our previous work.[22] We used Mason–Rice combining rules[23,24] for the hydroxide-carbonate cross-interactions (arithmetic mean for the size and geometric mean for the energy parameters). Carbonate was modeled as a flexible molecule, while hydroxide was kept rigid.

MD simulations were performed using the GROMACS simulation program, v.2018.[25,26] All simulations used the leapfrog (MD) algorithm with a time step of 1 fs. The van der Waals and real-space Coulomb interactions utilized a 1.0 nm cutoff. Particle-mesh Ewald summations were used to account for the long-range Coulomb interactions, and a standard van der Waals long-range correction was applied to the simulations of the dynamic properties. Because the two-phase simulations used for the surface tension calculations involve a non-homogeneous system, standard long-range corrections for van der Waals interaction were not employed. To account for this, surface tension was later corrected analytically following the method proposed by Mecke et al.[27] The simulations at constant temperature employed the canonical velocity rescale thermostat[28] and the constant pressure simulations employed the Parrinello–Rahman barostat.[29] All simulations (dynamic and interface properties) were performed on a system composed of 1000 cations and the matching number of hydroxide and carbonate ions required for charge neutrality. Finite-size effects in these electrolyte systems are expected to be minimal due to the effective screening of electrostatic interactions in ionic melts.[30] All uncertainties were estimated from five independent simulations.

Viscosity and Ionic Conductivity. In order to calculate the dynamic properties such as viscosity and ionic conductivity, the systems were first equilibrated for 5 ns in the *NPT* ensemble to determine the equilibrium volume at 1 bar. The systems were then equilibrated for 1 ns in the *NVT* ensemble to the correct temperature, and finally, a 5 ns production run was performed using the *NVE* ensemble so that the dynamics were not affected by the presence of a thermostat or barostat. To ensure that energy was conserved, GROMACS

https://dx.doi.org/10.1021/acs.jpcc.0c07295
J. Phys. Chem. C 2020, 124, 23532−23540

Table 1. Viscosity and Ionic Conductivity for Mixed Cation Carbonates Obtained from Simulations[a]

system	T (K)	η_{Sim}	η_{Exp}	$\Delta\eta$ (%)	σ_{Sim}	σ_{Exp}	$\Delta\sigma$ (%)
$Li_{0.8}K_{1.2}CO_3$	1103	6.08 ± 0.18	3.24	88	140 ± 5	202	−31
$Li_{1.0}K_{1.0}CO_3$	1098	6.64 ± 0.18	3.38	79	126 ± 2	206	−39
$Li_{1.2}K_{0.8}CO_3$	1096	6.93 ± 0.28	3.57	94	138 ± 8	237	−42
$Li_{0.8}Na_{1.2}CO_3$	921	15.4 ± 0.47			103 ± 3		
$Li_{1.0}Na_{1.0}CO_3$	1103	7.11 ± 0.18	4.12	73	190 ± 11	324	−41
$Li_{1.2}Na_{0.8}CO_3$	924	15.6 ± 0.32			113 ± 11		
$Na_{1.0}K_{1.0}CO_3$	1102	5.74 ± 0.17	3.95	45	146 ± 2	206	−29

[a]Viscosity, η (cP), percent deviation $\Delta\eta$ (= $100(\eta_{Sim} - \eta_{Exp})/\eta_{Exp}$), ionic conductivity σ (S/m), and percent deviation $\Delta\sigma$ (= $100(\sigma_{Sim} - \sigma_{Exp})/\sigma_{Exp}$). Uncertainties represent one standard error. For the remaining mixtures, the values are tabulated in Tables S1−S6. Experimental data are from ref 9.

was compiled with double precision (used only for dynamic property simulations).

The viscosity (η) and ionic conductivity (σ) were calculated using the Green−Kubo method as shown in eqs 1 and 2.[31−33]

$$\eta = \frac{V}{10kT}\int_0^\infty \boldsymbol{P}(0):\boldsymbol{P}(t)\,\mathrm{d}t \tag{1}$$

$$\sigma = \frac{1}{3VkT}\int_0^\infty \boldsymbol{j}(0)\cdot\boldsymbol{j}(t)\,\mathrm{d}t \tag{2}$$

Here, V is the simulation volume, k is the Boltzmann constant, and T is the temperature. Box sizes in these simulations were in the range of 3.25−3.65 nm. The pressure tensor, $\boldsymbol{P}$, and electric current vector, $\boldsymbol{j}$, were stored at every simulation time step (1 fs) to capture the short-term behavior of the correlation functions.

The pressure tensor autocorrelation function was calculated for 30 ps intervals with starting points separated by 0.1 ps. As can be seen in Figure S1, the integral in eq 1 converged within 20 ps. Therefore, the viscosity values were taken as the average value of the integral between 20 and 30 ps. The current autocorrelation function was calculated for 3 ps intervals with starting points separated by 0.1 ps. As can be seen in Figure S2, the integral in eq 2 converged within 1 ps. Thus, the conductivity values were taken from the average value of the integral between 1 and 3 ps.

Surface Tension. The calculations of surface tension used a two-phase system in the *NVT* ensemble. A pre-equilibrated configuration of the bulk liquid in the *NPT* ensemble was taken. The length of the simulation box along the z-axis was increased to 10.5 nm (or approximately 3 times the x and y box lengths) to generate two liquid−vapor interfaces. The simulations were then run for 20 ns to equilibrate the systems. This was followed by a 5 ns production run during which the diagonal elements of the pressure tensor were stored every 0.1 ps.

Surface tension was calculated from a two-phase simulation, in which the molten carbonate−hydroxide is in equilibrium with its vapor (essentially vacuum under the conditions studied). The surface tension (γ_0, without long-range correction) can be found from the difference between the pressure tensor element perpendicular to the interface (P_{zz}) and the elements parallel to the interface (P_{xx} and P_{yy}), as shown in eq 3.[34]

$$\gamma_0 = \frac{L_z}{2}\left[P_{zz} - \frac{1}{2}(P_{xx} + P_{yy})\right] \tag{3}$$

L_z is the length of simulation box in the direction parallel to the interface normal, set here as the z-axis. Since the simulation was not of a homogeneous system, the standard long-range corrections for the $\frac{1}{r^6}$ van der Waals interaction cannot be used. Instead, the simulation was run without any correction term for the long-range van der Waals interactions, and the surface tension was corrected analytically. The surface tension correction was based off the correction term used in Mecke et al.,[27] but modified to use the average simulation density profile of each atom type (having a nonzero van der Waals interaction parameter). The correction term is given in eq 4.

$$\gamma_{LRC} = \frac{\pi}{4}\sum_i^{N_{type}}\sum_j^{N_{type}}\int_{-L_z}^{L_z} dz\int_{r_c}^{\infty}\mathrm{d}r\int_0^{\pi}\mathrm{d}\phi\; r^3 u'_{i,j}(r)$$
$$(1 - 3\cos^2\phi)\sin\phi\,\langle\rho_i(z)\rangle\langle\rho_j(z + r\cos\phi)\rangle \tag{4}$$

Here, r_c is the cutoff, $u'_{i,j}(r)$ is the derivative of the van der Waals (in this case Buckingham) potential between atoms i and j, and $\rho_i(z)$ is the density profile of atom i. The sum of γ_0 and γ_{LRC} yields the total surface tension (γ_{Sim}) from simulation. The running average surface tension profiles in the unary salts and eutectic mixtures are plotted in Figure S11. These profiles clearly show that the computed surface tension is well-converged within the 5 ns production trajectories.

RESULTS AND DISCUSSION

Viscosity and Ionic Conductivity. Tables 1 and S1−S6 provide calculated viscosity and ionic conductivity of the alkali-metal carbonate−hydroxide cation mixtures. A comparison of these collective quantities acquired from our simulations with existing experimental values[9] are shown in Figures 1a and 2a, respectively. The computed viscosity is always higher than that of experiments, while the ionic conductivity from our simulations is always lower than that from experiments. Overall, the estimated values are on average 36% lower for conductivity (with a standard deviation of 5%) and 76% higher for viscosity (with a standard deviation of 17%). Both these deviations indicate that the predicted dynamics are slower than they should be and follow trends similar to those observed in pure carbonate and hydroxide salts (using the same set of force field parameters) reported in our earlier work.[22] These differences in the collective transport properties can be attributed to the use of full charges (−2e for carbonate, −1e for hydroxide, and +1e for alkali-metal cations) in the present force field, and a similar behavior has been manifested previously for both ionic liquids[35] and electrolyte solutions.[36] More importantly, since the deviations from experiments are consistent across different systems, conclusions on relative trends in dynamic properties should still hold true.

https://dx.doi.org/10.1021/acs.jpcc.0c07295
J. Phys. Chem. C 2020, 124, 23532−23540

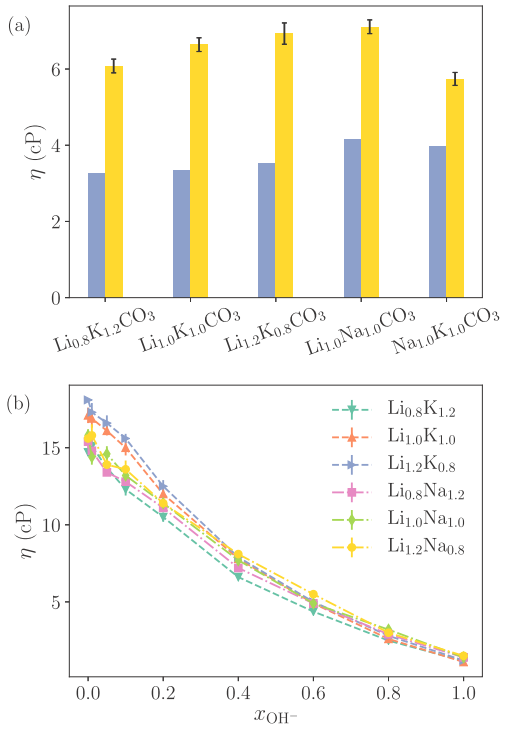

Figure 1. (a) Simulated (yellow) and experimental (gray) viscosity of mixed alkali-metal cation carbonate electrolytes. (b) Viscosity as a function of hydroxide mole fraction in molten alkali-metal carbonate−hydroxide mixtures obtained from simulation at 923.15 K. Values of viscosities are also tabulated in Table 1.

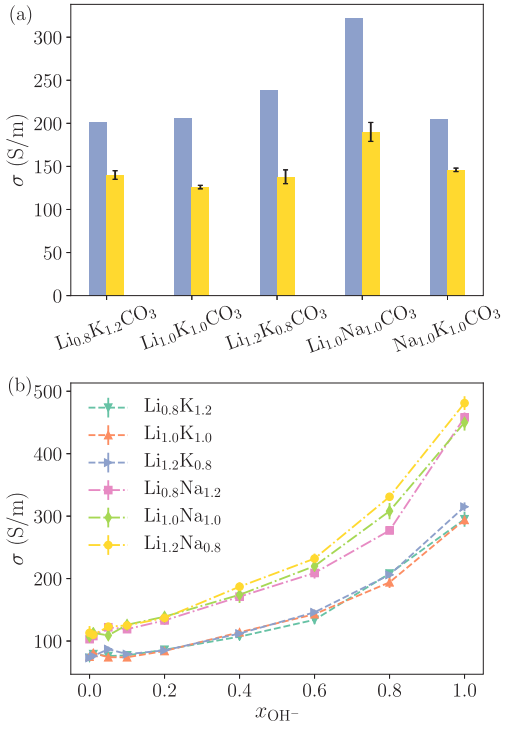

Figure 2. (a) Simulated (yellow) and experimental (gray) ionic conductivity of mixed alkali-metal cation carbonate electrolytes. (b) Ionic conductivity as a function of hydroxide mole fraction in molten alkali-metal carbonate−hydroxide mixtures obtained from simulations at 923.15 K. Values of ionic conductivities are also tabulated in Table 1.

Figures 1b and 2b show the computed viscosity and ionic conductivity, respectively, in the studied carbonate−hydroxide melts as a function of hydroxide mole fractions. In general, we observe a reduction in the viscosity upon an increase in the hydroxide mole fraction (see Figure 1). On the contrary, a higher hydroxide concentration results in an increase in the ionic conductivity of the salts (see Figure 2). Importantly, the presence of hydroxide in the electrolyte exhibits a larger impact on viscosity than ionic conductivity at low hydroxide concentrations while the opposite occurs at high hydroxide concentrations, as shown in Figures 1b and 2b. It is worth noting that MCFCs operate in the low hydroxide concentration regime where we observe that a 20% increase in the hydroxide mole fraction yields a larger increase in the ionic conductivity of Li−Na mixtures (on average 26%) than that of Li−K mixtures (on average 15%).

Furthermore, we have investigated the impact of the change in cation composition on the ionic conductivity and the viscosity of these Li-based mixed cation electrolytes. In general, inclusion of more Li^+ in the melt results in an increase in the viscosity of both Li−K and Li−Na salts, a trend which may seem counterintuitive. To rationalize this trend, we examined the cation−cation velocity autocorrelation functions in Li−K and Li−Na carbonate−hydroxide (60:40) mixtures. The results are shown in Figure S3. Velocity autocorrelation functions (VACFs) reveal how the initial dynamical information on an ion is lost by collisions with its neighboring ions. As is evident from Figure S3, both Na^+ and K^+ have fewer and less stable anions in their solvation shells compared to those in Li^+. The Li^+ ion, on the contrary, retains a more strongly bound and stable solvation shell of anions indicated by a deeper first minimum in the VACF (Figure S3). In fact, the Li^+ ACFs show the deepest first minimum of the three cations. This indicates that the anion cage within which the cation rattles and undergoes regular collisions with neighboring cages is strongest for Li^+. This is likely the reason for the increase in viscosity at higher Li^+ concentrations in the electrolyte.

On the basis of the trend observed for the viscosity of these cation mixtures, it might be expected that there would be an increase in the ionic conductivity of these salts upon an increase in either Na^+ or K^+ cation fraction. However, the computed conductivities (Figure 2b) show the opposite order: Higher ionic conductivity is observed with increasing Li^+ concentration. The switch in the ionic conductivity order (as opposed to the order expected from the viscosity trend) is present in both the Li−K and Li−Na carbonate−hydroxide electrolytes. However, as shown in Figure S4, the effect is more visible in the Li−Na mixtures. A similar negative correlation between ionic conductivity and cation size was also reported in the MD simulations of molten alkali-metal carbonates by Desmaele et al.[21] In order to interpret this anomalous order in the ionic conductivity, we examined the cation−anion cross-current correlation functions that are shown in Figure 3. These correlation functions provide insight into the momentum transfer between ions.[37] If the movement of a given ion is on average in the same direction as that of another ion, then the integration of this correlation function becomes positive. If the motion of the other ion is in the opposite direction, then it becomes negative, and the integral of this correlation yields zero when there is no relation in the motion of the two ions.[38] As we can see in Figure 3, both Na^+−anion and K^+−anion correlation functions are consistently more positive than that of the corresponding Li^+−anion values. Also, the former

https://dx.doi.org/10.1021/acs.jpcc.0c07295
J. Phys. Chem. C 2020, 124, 23532−23540

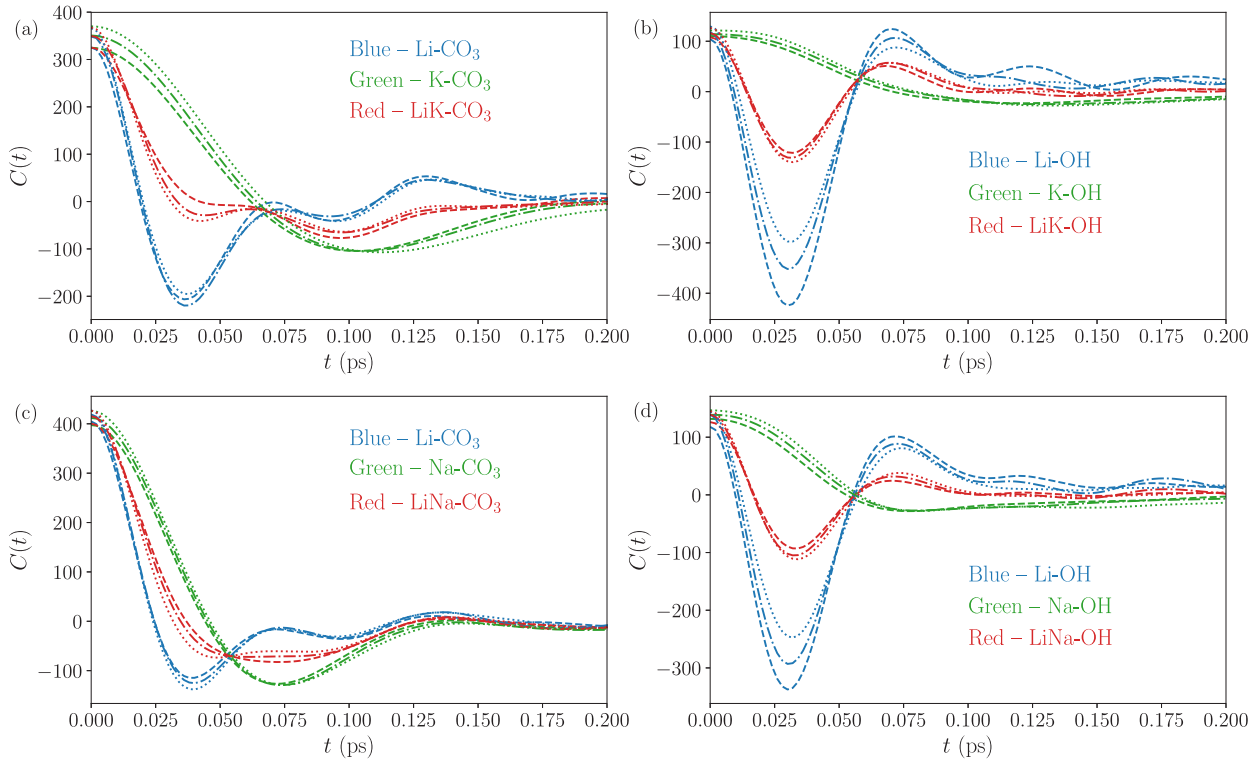

Figure 3. Normalized cation−anion cross-current correlation functions in (a, b) Li−K and (c, d) Li−Na carbonate/hydroxide (60:40) eutectic mixtures at 923.15 K. Dashed lines, dashed and dotted lines, and dotted lines represent $Li_{0.8}$, $Li_{1.0}$, and $Li_{1.2}$ fractions in the cation mixtures, respectively.

Table 2. Surface Tension for Molten Carbonate Salts and Cation Mixtures from Experiment[9] versus Simulations[a]

system	T (K)	γ_0	γ_{LRC}	γ_{Sim}	γ_{Exp}	$\Delta\gamma$ (%)
Li_2CO_3	1023.15	266.9	6.9	273.8 ± 1.5	243	13
Na_2CO_3	1178.15	213.0	4.5	217.5 ± 1.3	169	29
K_2CO_3	1143.15	180.9	7.8	188.7 ± 0.5	211	−11
$Li_{1.0}K_{1.0}CO_3$	923.15	210.9	8.9	219.8 ± 1.3	193	14
$Li_{1.0}Na_{1.0}CO_3$	923.15	241.8	6.0	247.8 ± 2.8	239	4

[a]Short-range surface tensions, γ_0 (mN/m), long-range corrections, γ_{LRC} (mN/m), their combined values, γ_{Sim} (mN/m), and percent deviations, $\Delta\gamma$ ($\Delta\gamma = 100(\gamma_{Sim} - \gamma_{Exp})/\gamma_{Exp}$). Uncertainties represent one standard error. For the remaining pure salts and mixtures, values are tabulated in Tables S8−S14.

correlations decay to zero at a longer time scale compared to that of the Li^+−anion results. The integral of these correlation functions is shown in Figure S5. As expected from Figure 3, the magnitudes of these integrals are found to be positive for both the Na^+−anion and K^+−anion correlation functions. However, for the Li^+−anion correlation function, the integrals are close to zero or negative (Figure S5). These observations certainly demonstrate that both carbonate and hydroxide are more correlated with Na^+ and K^+ than they are with Li^+. In other words, the anion and cations move in a concerted, pairwise manner (i.e., they have the same direction of center of mass velocity) when more Na^+ or K^+ is present in the electrolyte. Although this pairwise ion motion contributes to the respective ion diffusion, it does not contribute to the total ionic conductivity of the system. As a consequence, we observe an overall decrease in ionic conductivity with higher concentrations of either Na^+ or K^+.

In addition, in Table S7 we have tabulated the ionic conductivity calculated using the Nernst−Einstein equation[33] for a few representative mixtures. The Nernst−Einstein conductivity is almost within the uncertainty of the Green−Kubo values and shows similar trends, indicating that the Nernst−Einstein equation is a good method for estimating the conductivity of these ionic melts. The Nernst−Einstein equation neglects ion−ion correlations but still has an increase in conductivity with more Li^+. This increase in conductivity is driven by the Li^+ diffusion coefficient which increases with Li^+ concentration even as the viscosity increases and the diffusion coefficients of all other ions decrease. Therefore, both the faster diffusion of Li^+ and the weaker ion−ion correlations at higher Li^+ concentrations contribute to the increased conductivity.

Surface Tension. Tables 2 and S8−S14 provide the computed surface tension results including the long-range corrections, γ_{LRC}, of the unary salts and eutectic mixtures. The computed values are compared against available experimental values[9] in Figure 4a. In general, the estimated surface tensions from our simulations show good agreement with experimental measurements (an average difference of 14% with a standard deviation of 8%). Desmaele et al.[21] also reported surface tensions in molten carbonates calculated using a scaled-charge force field. However, their results indicated a systematic

https://dx.doi.org/10.1021/acs.jpcc.0c07295
J. Phys. Chem. C 2020, 124, 23532−23540

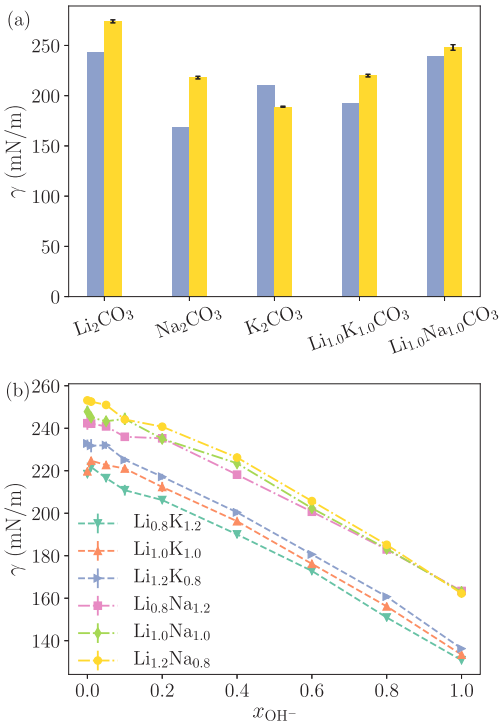

Figure 4. (a) Simulated (yellow) and experimental (gray) surface tensions in molten alkali-metal carbonate unary and eutectic electrolytes. (b) Surface tension as a function of hydroxide mole fraction in molten alkali-metal carbonate−hydroxide cation mixtures obtained from simulations at 923.15 K. Values of surface tensions are also tabulated in Table 2.

overestimation of experimental measurements by 15−20%. It is worth noting that the force field employed by Desmaele et al.[21] describes the transport properties (ionic conductivity and viscosity) with better accuracy than the present force field, chiefly because in the former force field the electronic polarization is captured effectively by scaling the ion charge by a factor of 0.82101. Previous reports on the two-phase simulations of liquid metals suggested the significance of incorporating experimental vapor−liquid surface tension values in the fitting procedure of classical force fields.[39] They proposed that inclusion of experimental values as part of the optimization procedure would result in the accurate prediction of surface tension from simulations. However, the resultant computational cost would be too demanding and certainly a downside of this proposed approach. In the present work, the better agreement in the predicted surface tension when compared to the viscosity and/or the ionic conductivity is likely due to the correct liquid phase energetics of the force field since the enthalpy of liquid was included as one of the objective functions during parametrization.[22]

Figure 4b shows the order in the computed surface tension in the studied carbonate−hydroxide cation mixtures as a function of hydroxide composition. In general, we observe a decreasing trend in the surface tension with an increase in the hydroxide concentration in carbonate−hydroxide mixtures. In contrast, replacing a larger cation (Na^+ or K^+) by a smaller cation (Li^+) results in an increase in surface tension. Thus, we find that the surface tension increases when the asymmetry of size between the cation and the anion increases.[40] A similar trend in the surface tension of pure molten carbonates was also reported by Desmaele et al.[21]

To investigate the liquid−vapor interface structure in these electrolytes, we have further explored the density profiles of different atom types. These density profiles are shown in Figures 5 and S6−S10. The density profiles are found to be flat in the bulk liquid regions, as expected, showing that the two-phase morphology is well-equilibrated. We observed a number of interesting buildups of ions near the interface in these molten salts. In the unary and binary carbonate systems (Figures 5a,b, S6, and S8), the larger/heavier cations (Na^+ or K^+) prefer the interface more than the smaller/lighter Li^+ ions, the latter of which points more toward the bulk. However, the situation becomes opposite in the binary hydroxide and

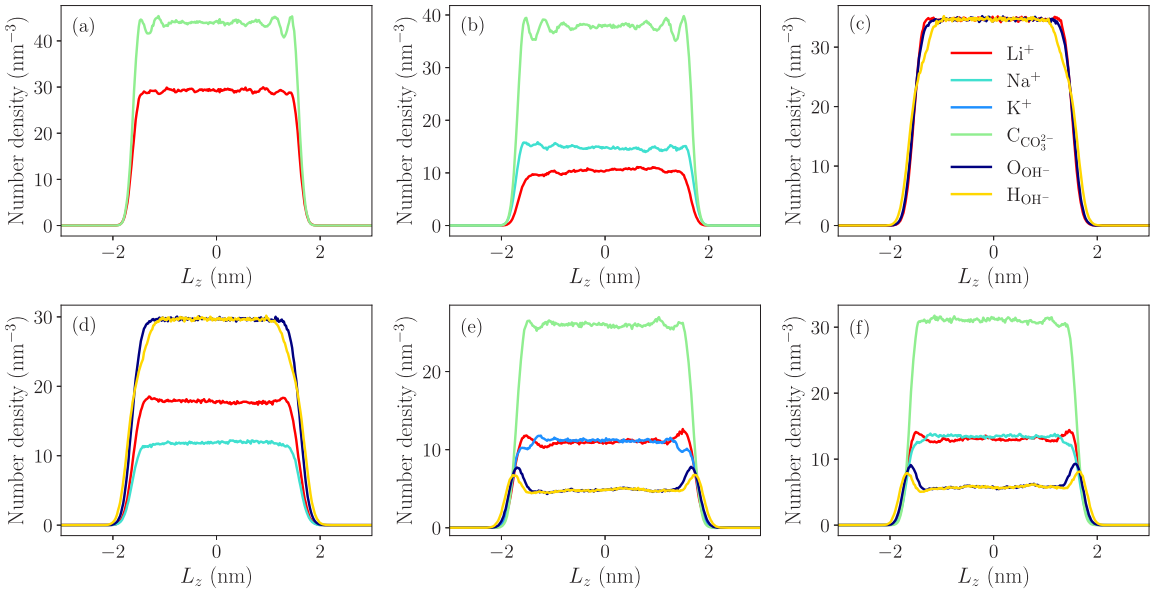

Figure 5. Density profiles of atom types with non-zero van der Waals interactions in (a) Li_2CO_3, (b) $Li_{0.8}Na_{1.2}CO_3$, (c) LiOH, (d) $Li_{1.2}Na_{0.8}OH$, (e) $Li_{1.0}K_{1.0}CO_3OH$, and (f) $Li_{1.0}Na_{1.0}CO_3OH$. The carbonate/hydroxide ratio in (e) and (f) are 0.6/0.4. Similar profiles for the remaining systems are provided in Figures S6−S10.

https://dx.doi.org/10.1021/acs.jpcc.0c07295
J. Phys. Chem. C 2020, 124, 23532−23540

carbonate−hydroxide cation mixture systems (Figures 5d,e,f, S9, and S10), where we see the accumulation of smaller/lighter Li^+ ion more toward the interface and larger/heavier Na^+ or K^+ ions far from the interface. However, when we compare the buildups of anions in carbonate−hydroxide cation mixtures (Figures 5e,f and S10), we find a clear preference of the hydroxide to be closer to the interface than the carbonate. The accumulation of more hydroxide near the interface is independent of the hydroxide composition in these carbonate−hydroxide cation mixtures as shown in Figure S10. A likely reason for this phenomenon could be the difference in polarity between these two anions. Carbonate (CO_3^{2-}), a symmetric anion with zero dipole moment (due to its D_{3h} symmetry), points away from the interface; in contrast, hydroxide, a more polar species with large dipole moment (1.49 D at the MP2/aug-cc-pVQZ level of theory), moves toward the interface. Since hydroxide is favored more at the interface than the carbonate, the switch from a larger cation (Na^+ or K^+) to a smaller cation (Li^+) being present near the interface in binary hydroxide and carbonate−hydroxide cation mixtures can be explained in terms of the hard−soft acid base (HSAB) theory.[41−43] The theory states that hard acids prefer to bond with hard bases, and correspondingly soft acids prefer to bond with soft bases. In HSAB theory, OH^- is considered a hard anion while CO_3^{2-} is significantly softer. Thus, Li^+, a smaller and harder cation, is pulled toward the interface by the harder anion, OH^-. Melts with carbonate have larger/softer cations near the interface, while melts with hydroxide have smaller/harder cations at the interface. Interestingly, we also observed a reversal in the direction of O−H bond in hydroxide anion toward the interface. In the unary and binary hydroxide systems, the hydroxide hydrogen tends to be far from the interface as shown in Figures 5c,d, S7, and S9. On the contrary, the direction alters in the carbonate−hydroxide cation mixtures (Figures 5e,f and S10), where the hydroxide hydrogen is found to be closer to the interface.

CONCLUSIONS

In this work, we report a systematic study of interfacial (surface tension) and transport properties (viscosity and ionic conductivity) of molten alkali carbonates, hydroxides, and carbonate−hydroxide mixtures with at a variety of Li-based binary alkali cation compositions. For this purpose, we employed a recently developed classical force field, reported in one of our earlier publications.[22] Although the primary objective of the present force field was to accurately predict liquid phase chemical potentials of pure molten carbonate and hydroxide salts, it was shown that the parameters can be extended to the molten carbonate−hydroxide mixtures by using standard combining rules.

Our current simulations yielded consistently higher viscosity (by an average 76%) and lower ionic conductivity (by an average 36%) than what was obtained from experiments. Nevertheless, the computed values show considerable promise in correctly predicting the relative trends in these dynamic properties. The discrepancy in the estimated transport properties is fully expected due to the use of full charges on the ions, a trend that has been confirmed previously for both ionic liquids[35] and electrolyte solutions.[36]

The simulated results provide us with important insights into the impact of the change in the hydroxide and cation compositions on the dynamic properties of these alkali carbonate melts. Overall, we observe a consistent decrease in viscosity and increase in conductivity upon an increase in hydroxide concentration. In contrast, inclusion of more Li^+ in the electrolyte exhibits an increase in both viscosity and ionic conductivity of these salts, an observation which may seem counterintuitive. We rationalize this by showing that Li^+ ions maintain a more stable solvation shell of anions than that of either Na^+ or K^+ ions, as indicated by a deeper first minimum in the velocity autocorrelation function. The stronger anion cage around Li^+ ions explains the observed trends in the viscosity as a function of Li^+ composition in the melts. Conversely, the cation−anion cross-current correlation functions reveal that both Na^+ and K^+ ions exhibit more correlated (pairwise) motion with counter-anions than that of Li^+ ions thus accounting for the drop in ionic conductivity with increasing concentrations of either Na^+ or K^+ in the melt.

Although the computed values of surface tension show rather small differences when compared with experimental results (an average difference of 14% with a standard deviation of 8%), the discrepancy is moderate, as also observed in previous simulation studies dealing with molten carbonates.[21] The calculated values show a negative correlation with hydroxide and a positive correlation with Li^+ concentrations in the carbonate−hydroxide cation mixtures. Overall, the surface tension increases with the asymmetry between cation and anion sizes,[40] an order also observed in previous surface tension simulations of pure molten carbonates.[21] The density profiles of these interfacial simulations suggest that hydroxide occupies the interface region more than carbonate, which was explained by differences in their dipole moments. Also, in the presence of hydroxide (smaller/harder) anions in the electrolyte, the smaller (harder) cation, Li^+, is more favored at the interface than is a larger cation, Na^+ or K^+. Experimental probing of these system using electron microscopy[44] would be necessary to verify the observed interfacial structures. We believe that these simulation results will guide future experimental studies into the complex nature of molten carbonates, and can also aid in the development of molten carbonate fuel cell electrolytes.

ASSOCIATED CONTENT

Supporting Information

The Supporting Information is available free of charge at https://pubs.acs.org/doi/10.1021/acs.jpcc.0c07295.

Running integrals of ionic conductivity and shear viscosity, velocity autocorrelation functions, viscosity and ionic conductivity as a function of hydroxide mole fraction, integrals of cation−anion cross-current correlation functions, ionic conductivity and viscosity in molten salts, number density profiles in molten salts, running averages of surface tension, and surface tensions in molten salts (PDF)

AUTHOR INFORMATION

Corresponding Authors

Lucas Koziol − *ExxonMobil Research and Engineering Co., Annandale, New Jersey 08801, United States*; Email: lucas.koziol@exxonmobil.com

Athanassios Z. Panagiotopoulos − *Department of Chemical and Biological Engineering, Princeton University, Princeton, New Jersey 08544, United States*; orcid.org/0000-0002-8152-6615; Email: azp@princeton.edu

Authors

Anirban Mondal − *Department of Chemical and Biological Engineering, Princeton University, Princeton, New Jersey 08544, United States;* orcid.org/0000-0003-3029-8840

Jeffrey M. Young − *Department of Chemical and Biological Engineering, Princeton University, Princeton, New Jersey 08544, United States;* orcid.org/0000-0001-8879-5132

Timothy A. Barckholtz − *ExxonMobil Research and Engineering Co., Annandale, New Jersey 08801, United States*

Gabor Kiss − *ExxonMobil Research and Engineering Co., Annandale, New Jersey 08801, United States*

Complete contact information is available at: https://pubs.acs.org/10.1021/acs.jpcc.0c07295

Notes

The authors declare the following competing financial interest(s): T.A.B., G.K., and L.K., are all employees of ExxonMobil Research and Engineering Co., currently working on applications of MCFCs in the industrial and power sectors.

■ ACKNOWLEDGMENTS

Financial support for this work was provided by ExxonMobil Research and Engineering Co., under agreement EM09125.A1, and by the Office of Basic Energy Sciences, U.S. Department of Energy, under Award DE-SC0002128. Computing resources were provided by Princeton Research Computing.

■ REFERENCES

(1) Serrano-López, R.; Fradera, J.; Cuesta-López, S. Molten Salts Database for Energy Applications. *Chem. Eng. Process.* **2013**, *73*, 87−102.

(2) Tomczyk, P. MCFC Versus Other Fuel Cells-Characteristics, Technologies and Prospects. *J. Power Sources* **2006**, *160*, 858−862.

(3) Caprile, L.; Passalacqua, B.; Torazza, A. Carbon Capture: Energy Wasting Technologies or the MCFCs Challenge? *Int. J. Hydrogen Energy* **2011**, *36*, 10269−10277.

(4) Wee, J.-H. Carbon Dioxide Emission Reduction Using Molten Carbonate Fuel Cell Systems. *Renewable Sustainable Energy Rev.* **2014**, *32*, 178−191.

(5) Discepoli, G.; Cinti, G.; Desideri, U.; Penchini, D.; Proietti, S. Carbon Capture with Molten Carbonate Fuel Cells: Experimental Tests and Fuel Cell Performance Assessment. *Int. J. Greenhouse Gas Control* **2012**, *9*, 372−384.

(6) Selman, J. R.; Chen, C.-C. Scientific and Technical Maturity of Molten Carbonate Technology. *Int. J. Hydrogen Energy* **2012**, *37*, 19280−19288.

(7) Young, J. M.; Mondal, A.; Barckholtz, T. A.; Kiss, G.; Koziol, L.; Panagiotopoulos, A. Z. Predicting Chemical Reaction Equilibria in Molten Carbonate Fuel Cells via Molecular Simulations. *AIChE J.* **2020**, e16988.

(8) Rosen, J.; Geary, T.; Hilmi, A.; Blanco-Gutierrez, R.; Yuh, C.-Y.; Pereira, C. S.; Han, L.; Johnson, R. A.; Willman, C. A.; Ghezel-Ayagh, H.; et al. Performance of Molten Carbonate Fuel Cells for Deep CO_2 Capture from Natural Gas Combined Cycle Flue Gas. *J. Electrochem. Soc.* **2020**, *167*, 064505.

(9) Janz, G. J. Thermodynamic and Transport Properties for Molten Salts: Correlation Equations for Critically Evaluated Density, Surface Tension, Electrical Conductance, and Viscosity Data. *J. Phys. Chem. Ref. Data* **1988**, *17*, 159−266.

(10) Witt, W. C.; Del Rio, B. G.; Dieterich, J. M.; Carter, E. A. Orbital-Free Density Functional Theory for Materials Research. *J. Mater. Res.* **2018**, *33*, 777−795.

(11) Chen, M.; Vella, J. R.; Panagiotopoulos, A. Z.; Debenedetti, P. G.; Stillinger, F. H.; Carter, E. A. Liquid Li Structure and Dynamics: A Comparison Between OFDFT and Second Nearest-Neighbor Embedded-Atom Method. *AIChE J.* **2015**, *61*, 2841−2853.

(12) Tissen, J. T.; Janssen, G. J. Molecular-Dynamics Simulation of Molten Alkali Carbonates. *Mol. Phys.* **1990**, *71*, 413−426.

(13) Habasaki, J. Molecular Dynamics Simulation of Molten Li_2CO_3 and Na_2CO_3. *Mol. Phys.* **1990**, *69*, 115−128.

(14) Koishi, T.; Kawase, S.; Tamaki, S.; Ebisuzaki, T. Computer Simulation of Molten Li_2CO_3-K_2CO_3 Mixtures. *J. Phys. Soc. Jpn.* **2000**, *69*, 3291−3296.

(15) Costa, M. F. Molecular Dynamics of Molten Li_2CO_3-K_2CO_3. *J. Mol. Liq.* **2008**, *138*, 61−68.

(16) Ottochian, A.; Ricca, C.; Labat, F.; Adamo, C. Molecular Dynamics Simulations of a Lithium/Sodium Carbonate Mixture. *J. Mol. Model.* **2016**, *22*, 61.

(17) Ding, J.; Xie, W.; Wei, X.; Wang, W.; Lu, J.; Du, L. Molecular Dynamics Simulations of the Thermodynamic Properties and Local Structures on Molten Alkali Carbonate Na_2CO_3. *Int. J. Heat Mass Transfer* **2019**, *131*, 41−51.

(18) Ding, J.; Du, L.; Pan, G.; Lu, J.; Wei, X.; Li, J.; Wang, W.; Yan, J. Molecular Dynamics Simulations of the Thermodynamic Properties and Local Structures on Molten Alkali Carbonate K_2CO_3. *Appl. Energy* **2018**, *220*, 536−544.

(19) Vuilleumier, R.; Seitsonen, A.; Sator, N.; Guillot, B. Structure, Equation of State and Transport Properties of Molten Calcium Carbonate ($CaCO_3$) by Atomistic Simulations. *Geochim. Cosmochim. Acta* **2014**, *141*, 547−566.

(20) Corradini, D.; Coudert, F. X.; Vuilleumier, R. Insight into the Li_2CO_3-K_2CO_3 Eutectic Mixture from Classical Molecular Dynamics: Thermodynamics, Structure, and Dynamics. *J. Chem. Phys.* **2016**, *144*, 104507.

(21) Desmaele, E.; Sator, N.; Vuilleumier, R.; Guillot, B. Atomistic Simulations of Molten Carbonates: Thermodynamic and Transport Properties of the Li_2CO_3-Na_2CO_3-K_2CO_3 System. *J. Chem. Phys.* **2019**, *150*, 094504.

(22) Mondal, A.; Young, J. M.; Barckholtz, T. A.; Kiss, G.; Koziol, L.; Panagiotopoulos, A. Z. Genetic Algorithm Driven Force Field Parameterization for Molten Alkali-Metal Carbonate and Hydroxide Salts. *J. Chem. Theory Comput.* **2020**, *16*, 5736−5746.

(23) Mason, E. A.; Rice, W. E. The Intermolecular Potentials of Helium and Hydrogen. *J. Chem. Phys.* **1954**, *22*, 522−535.

(24) Mirskaya, K. V. Combining Rules for Interatomic Potential Functions of Buckingham Form. *Tetrahedron* **1973**, *29*, 679−682.

(25) Hess, B.; Kutzner, C.; Van Der Spoel, D.; Lindahl, E. GROMACS 4: Algorithms for Highly Efficient, Load-Balanced, and Scalable Molecular Simulation. *J. Chem. Theory Comput.* **2008**, *4*, 435−447.

(26) Pronk, S.; Páll, S.; Schulz, R.; Larsson, P.; Bjelkmar, P.; Apostolov, R.; Shirts, M. R.; Smith, J. C.; Kasson, P. M.; van der Spoel, D.; et al. GROMACS 4.5: A High-Throughput and Highly Parallel Open Source Molecular Simulation Toolkit. *Bioinformatics* **2013**, *29*, 845−854.

(27) Mecke, M.; Winkelmann, J.; Fischer, J. Molecular Dynamics Simulation of the Liquid − Vapor Interface: The Lennard-Jones Fluid. *J. Chem. Phys.* **1997**, *107*, 9264.

(28) Bussi, G.; Donadio, D.; Parrinello, M. Canonical Sampling through Velocity Rescaling. *J. Chem. Phys.* **2007**, *126*, 014101.

(29) Parrinello, M.; Rahman, A. Polymorphic Transitions in Single Crystals: A New Molecular Dynamics Method. *J. Appl. Phys.* **1981**, *52*, 7182−7190.

(30) Young, J. M.; Panagiotopoulos, A. Z. System-Size Dependence of Electrolyte Activity Coefficients in Molecular Simulations. *J. Phys. Chem. B* **2018**, *122*, 3330−3338.

(31) Harada, M.; Yamanaka, A.; Tanigaki, M.; Tada, Y. Mass and Size Effects on the Transport Properties of Molten Salts. *J. Chem. Phys.* **1982**, *76*, 1550−1556.

(32) Daivis, P. J.; Evans, D. J. Comparison of Constant Pressure and Constant Volume Nonequilibrium Simulations of Sheared Model Decane. *J. Chem. Phys.* **1994**, *100*, 541−547.

(33) Hansen, J.-P.; McDonald, I. R. *Theory of Simple Liquids: With Applications to Soft Matter*, 4th ed.; Academic Press: New York, 2013.

(34) Rowlinson, J. S.; Widom, B. *Molecular Theory of Capillarity*; Clarendon Press: New York, 1982.
(35) Youngs, T. G.; Hardacre, C. Application of Static Charge Transfer within an Ionic-Liquid Force Field and its Effect on Structure and Dynamics. *ChemPhysChem* **2008**, *9*, 1548−1558.
(36) Yue, S.; Panagiotopoulos, A. Z. Dynamic Properties of Aqueous Electrolyte Solutions from Non-Polarisable, Polarisable, and Scaled-Charge Models. *Mol. Phys.* **2019**, *117*, 3538−3549.
(37) Balucani, U.; Vallauri, R.; Murthy, C. S.; Gaskell, T.; Woolfson, M. S. Velocity Correlations, Cooperative Effects and Relative Diffusion in Simple Liquids. *J. Phys. C: Solid State Phys.* **1983**, *16*, 5605−5616.
(38) Yoon, T. J.; Patel, L. A.; Vigil, M. J.; Maerzke, K. A.; Findikoglu, A. T.; Currier, R. P. Electrical Conductivity, Ion Pairing, and Ion Self-Diffusion in Aqueous NaCl Solutions at Elevated Temperatures and Pressures. *J. Chem. Phys.* **2019**, *151*, 224504.
(39) Vella, J. R.; Chen, M.; Stillinger, F. H.; Carter, E. A.; Debenedetti, P. G.; Panagiotopoulos, A. Z. Structural and Dynamic Properties of Liquid Tin from a New Modified Embedded-Atom Method Force Field. *Phys. Rev. B: Condens. Matter Mater. Phys.* **2017**, *95*, 064202.
(40) González-Melchor, M.; Orea, P.; López-Lemus, J.; Bresme, F.; Alejandre, J. Stress Anisotropy Induced by Periodic Boundary Conditions. *J. Chem. Phys.* **2005**, *122*, 094503.
(41) Pearson, R. G. Hard and Soft Acids and Bases. *J. Am. Chem. Soc.* **1963**, *85*, 3533−3539.
(42) Pearson, R. G. Hard and Soft Acids and Bases, HSAB, Part I: Fundamental Principles. *J. Chem. Educ.* **1968**, *45*, 581−587.
(43) Pearson, R. G. Hard and Soft Acids and Bases, HSAB, Part II: Underlying Theories. *J. Chem. Educ.* **1968**, *45*, 643−648.
(44) Ren, A.; Lu, D.; Wong, E.; Hauwiller, M. R.; Alivisatos, A. P.; Ren, G. Real-Time Observation of Dynamic Structure of Liquid-Vapor Interface at Nanometer Resolution in Electron Irradiated Sodium Chloride Crystals. *Sci. Rep.* **2020**, *10*, 8596.

https://dx.doi.org/10.1021/acs.jpcc.0c07295
J. Phys. Chem. C 2020, 124, 23532−23540